separations

MDPI

Article

Aqueous 2-Ethyl-4-methylimidazole Solution for Efficient CO_2 Separation and Purification

Xingtian Zhang [1,2,3], Jun Wu [4], Xiaoxiao Lu [3], Yefeng Yang [1,*], Li Gu [2,*] and Xuebo Cao [3,*]

[1] School of Materials Science and Engineering, Zhejiang Sci-Tech University, Hangzhou 310018, China
[2] School of Materials and Textile Engineering, Jiaxing University, Jiaxing 314001, China
[3] College of Biological, Chemical Sciences and Engineering, Jiaxing University, Jiaxing 314001, China
[4] College of Advanced Materials Engineering, Jiaxing Nanhu University, Jiaxing 314001, China
* Correspondence: yangyf@zstu.edu.cn (Y.Y.); guli@zjxu.edu.cn (L.G.); xbcao@zjxu.edu.cn (X.C.); Tel.: +86-0573-83642712 (X.C.)

Abstract: Carbon capture and storage (CCS) technology is considered as one of the most effective short-term solutions in reducing atmospheric CO_2 concentrations. A key of CCS technology is to seek the absorbent with low cost, fast absorption rate, and high stability. In this study, we show that 2-ethyl-4-methylimidazole is particularly suitable for efficient CO_2 capture. The aqueous solution of 2-ethyl-4-methylimidazole displays a maximum CO_2 molar absorption capacity of 1.0 mol·mol^{-1} and the absorbed CO_2 can be completely released through heating the solution at a relatively low temperature (<100 °C). Stability tests show that the aqueous system is quite stable, with less than 10% loss of the molar absorption capacity after eight absorption–desorption cycles. Time-related *in-situ* attenuated total reflection infrared absorption spectroscopy and ^{13}C nuclear magnetic resonance spectroscopy studies reveal that the intermediates are HCO_3^- and H_2CO_3 in the process of CO_2 absorption–desorption. These intermediates are easily decomposed, which are responsible for the low CO_2 desorption temperature and high desorption efficiency of the system. Moreover, the aqueous solution of 2-ethyl-4-methylimidazole is able to separate and purify CO_2 from flue gas and even ambient air. Consequently, 2-ethyl-4-methylimidazole is a promising low-cost CO_2 absorbent for industrial implementation.

Keywords: CO_2 capture; 2-ethyl-4-methylimidazole; bicarbonate ion; absorption-desorption

Citation: Zhang, X.; Wu, J.; Lu, X.; Yang, Y.; Gu, L.; Cao, X. Aqueous 2-Ethyl-4-methylimidazole Solution for Efficient CO_2 Separation and Purification. *Separations* **2023**, *10*, 236. https://doi.org/10.3390/separations10040236

Academic Editor: Sohrab Zendehboudi

Received: 21 February 2023
Revised: 25 March 2023
Accepted: 26 March 2023
Published: 3 April 2023

1. Introduction

Since the industrial revolution, human-caused CO_2 emissions have increased exponentially [1]. Rising concentrations of CO_2 in the atmosphere contributes to the greenhouse effect, which makes the global temperature rise continuously [2,3]. The situation is likely to get worse in the future, as an expanding population and industrialization continue to produce CO_2 from the burning of fossil fuels. Since the 1970s, this anthropic influence has caused the global mean surface temperature (GMST) to rise at an average rate of 0.2 °C per decade [4]. In order to address this challenge, the Paris Agreement was signed by consensus in 2015, controlling the increase in global average temperature above the pre industrialization level and below 2 °C [5,6]. Carbon capture and storage (CCS) technology is considered as one of the most effective short-term solutions in the fight against global warming and plays a vital role in reducing atmospheric CO_2 concentrations [7–9]. To keep the targets set by the Paris agreement, about 1 billion tonnes of CO_2 must be captured each year and up to 16 billion tonnes stored by 2050 [10]. At the same time, CO_2 is considered to be a cheap C1 source, which can be directly used for the subsequent conversion of multi-carbon products after capture, so the early capture is particularly critical [11,12].

CO_2 capture is the most economical and feasible method to restrain carbon emissions from industrial point sources [13]. According to the current technical progress, amine chemisorbents, such as ethanolamine (MEA) [14,15], *N*-methyldiethanolamine (MDEA) [16],

and piperazine (PZ) [17], have fast absorption rate, high absorption capacity, and mild operating conditions, and are often used to capture CO_2, which is also one of the most mature CO_2 separation technologies at present [18–20]. Especially, aqueous solutions of MEA have been extensively studied in post-combustion CO_2 capture systems, and it is regarded as the benchmark for all CCS processes [14,15,21]. MEA has a strong affinity to CO_2, resulting in favorable absorption kinetics. However, this method has three major disadvantages: solvent degradation, equipment corrosion, and regeneration high energy consumption. The solvent regeneration process requires a lot of energy to decompose stable carbamate formed during CO_2 capture (temperature is about 120–140 °C), accounting for about 70–80% of the total cost of capture system [22–24]. Moreover, the most common impurity in industrial waste gas is O_2. In the presence of O_2, the absorbent containing amine is rapidly deactivated by the oxidation of amine [25–28]. There are many obstacles in using amine absorption method to capture CO_2 after combustion, which has become an unavoidable challenge for its large-scale commercial application. The affinity between the absorbent and CO_2 must be precisely regulated: if the interaction is too strong, the desorption energy will be great, whereas if the interaction is too weak, CO_2 will not be completely absorbed [29]. Therefore, it is of great significance to develop MEA alternatives with low energy loss and fast absorption rate.

Imidazole is an interesting class of basic heterocyclic compounds in nature. Its main use is as a precursor material for the synthesis of other more complex compounds [30], and it has not been widely used as an absorbent for CO_2 capture except for a few examples. Tomizaki et al. studied the reaction heat and vapor–liquid equilibrium of several imidazoles [31]. Evjen et al. investigated the CO_2 absorption capacity of polyalkylated imidazoles and found that these imidazole-based solvents can achieve high CO_2 absorption capacity [32]. Shannon et al. found that pure *N*-alkylimidazole has relatively low viscosity and density compared to its corresponding *N*-alkylimidazole-based ionic liquid [33]. Chen et al. measured the solubility of CO_2 in 5~30 wt% 2-methylimidazole aqueous solution at 293.15–313.15 K [34]. Lin et al. introduced imidazole into polyelectrolyte membrane as an alkaline group and showed a good CO_2 selective separation effect [35]. Yan et al. found that the introduction of imidazole improved the adsorption capacity and thermal stability of amine adsorbents [36]. Li et al. demonstrated that 1-methylimidazole is a phase separator that induces phase separation and an absorption promoter that increases the absorption rate [37]. Moreover, imidazole ionic liquids show good CO_2 absorption capacity [38]. Cheng et al. studied the CO_2 absorption mechanism by deep eutectic solvents based on ethylene glycol and protic ionic liquid ([MEAH][Im]), formed by monoethanolamine with imidazole [39]. Considering that imidazole-based compounds have low saturated vapor pressure and viscosity [40,41], excellent thermal and antioxidant stability [42–44], and low reaction heat [31], they should have potential for efficient and low-cost CO_2 capture.

In this work, we investigated the CO_2 absorption performance of a total of ten low-molecular-weight solid imidazoles. Of them, 2-ethyl-4-methylimidazole was found to be the optimum absorbent for CO_2 capture, as it presents the best CO_2 absorption performance on the basis of the large absorption capacity, fast absorption rate, relatively low desorption temperature (90 °C), and excellent cycle performance. The mechanism of CO_2 absorption–desorption was studied by time-related *in-situ* attenuated total reflection infrared absorption spectroscopy and ^{13}C nuclear magnetic resonance spectroscopy. Moreover, 2-ethyl-4-methylimidazole is capable of efficiently separating and purifying CO_2 from flue gas and ambient air.

2. Materials and Methods

2.1. Materials

All the imidazoles (reagent grade) studied in this work were obtained from commercial sources, which were provided by Macklin Reagent (Macklin Biochemical Co., Ltd., Shanghai, China). Ethanolamine was provided by Sinopharm Reagent (Sinopharm Chemical Reagent Co., Ltd., Shanghai, China). Deuterium oxide (99% wt %) used in nuclear magnetic

resonance spectroscopy experiments was purchased from Sinopharm Chemical Reagent Co., Ltd., Shanghai, China. The purity of CO_2, N_2, and O_2 is 99.99% vol %, provided by Zhejiang Nankai Gas Co., Ltd., Jiaxing, China. The deionized (DI) water was prepared by reverse osmosis ultra-pure water equipment (conductivity $\leq$ 0.1 μS/cm).

2.2. Absorption Experiment

The absorption experimental setup for CO_2 capture is diagrammatically described in Figure S1. The imidazole solid was dissolved in DI water and the aqueous solution is transferred to the bubbling reactor immersed in a water bath to keep the reaction temperature constant CO_2 gas bubbles into the reactor, and the unabsorbed CO_2 gas is discharged into the tail gas treatment bottle containing sodium hydroxide. The gas flow rate is controlled by the mass flowmeter, and the amount of CO_2 absorbed is quantified by gravimetric method [45–47]. All absorption experiments were conducted at atmospheric pressure. The temperature was controlled in the range of 25~60 °C. To avoid accidental absorption of CO_2 by the solution, all gas pipelines were blown with N_2 before the experiment was run. The weight difference of each measurement represents the amount of CO_2 absorbed by the solution. As long as the mass does not rise during continuous measurement, the balance of CO_2 absorption can be considered to be reached. The cumulative absorption of CO_2 can be calculated with Equation (1).

$$X = \frac{(m_t - m_0)/44.01}{m_l/M_m} \quad (1)$$

where X is the CO_2 molar absorption capacity ($mol_{CO_2} \cdot mol^{-1}{}_{imidazole}$), m_t the mass of the bubbling reactor after CO_2 capture (g), m_0 the mass of the bubbling reactor before CO_2 capture (g), m_l the mass of the imidazole (g), and M_m the molecular mass of the imidazole ($g \cdot mol^{-1}$).

2.3. Desorption Experiment

The desorption setup is similar to the absorption reaction setup. As shown in Figure S1b, the gas bubbling tube at the upper part of the reactor is changed into a condensing tube to recover the evaporated liquid returned to the reaction bottle to reduce solution loss. The released gas passes through the cooling device and drying pipe to remove excess water and then enters the gas flow monitor. When the monitored gas flow rate is 0 mL/min, it proves that the CO_2 gas is completely released. The tail of the device is a tail gas absorption bottle containing sodium hydroxide solution.

2.4. Flue Gas Capture

For CO_2 capture in flue gas, we developed a simplified CO_2 capture setup for separating and purifying CO_2 from the flue gas. First, ten gas bubbling reactors containing imidazole aqueous solution were connected in series to form the absorption setup (Figure S2a). CO_2 (15%) was mixed with N_2 (77%) and O_2 (8%) to obtain a synthetic flue gas. The synthetic flue gas was continuously feed to the setup and the gas stream at the outlet was monitored through on-line gas chromatograph. In the desorption stage, the solution loaded by CO_2 was transferred to a vacuum flask and heated at 90 °C to release the CO_2 (Figure S2b).

2.5. Direct Air Capture

As shown in Figure S3, in order to capture environmental CO_2 with a concentration of 400 ppm, imidazole aqueous solution was placed in a beaker and exposed to air. After several hours, the concentrated CO_2 was collected by heating the solution and detected by gas chromatography.

2.6. Characterization

The pH of the solution was determined by a ST2100/F pH meter (Ohaus, Pine Brook, MN, USA) equipped with a ST310 pH electrode (Ohaus, Pine Brook, USA). The conductivity of the solution was determined by a DDS-307A conductivity meter (INASE Scientific Instrument Co., Ltd., Shanghai, China). The viscosity of the solution was measured by the NDJ-9S digital display viscometer (Shanghai Gaozhi Precise Instrument Co., Ltd., Shanghai, China). Nuclear magnetic resonance spectroscopy (NMR) measurements performed on the nuclear magnetic resonance spectrometer (Bruker Avance III 400 MHz, Zurich, Switzerland) was used to determine the changes of solvents in the process of CO_2 absorption and desorption. The *in-situ* attenuated total reflection infrared absorption spectrometer (React IR 701 L, Mettler Toledo, Zurich, Switzerland) was used to study the absorption–desorption behavior of CO_2. The gas released during desorption was analyzed by gas chromatography (FULI GC9790 plus, Zhejiang Fuli Analytical Instruments Co., Ltd., Wenling, China) equipped with a flame ionization detector (FID) and methanation reactors. The gas chromatograph is calibrated using different concentrations of standard gases. High resolution mass spectrometry (HRMS) was recorded on Thermo Scientific Q Exactive spectrometer (Waltham, MA, USA) equipped with ESI source and data acquisition was performed using MassHunter software (MassHunter 10.0, Agilent, Santa Clara, CA, USA).

3. Results and Discussion

A total of ten low-molecular-weight solid imidazoles (Table S1) were selected as the absorbents for CO_2 capture. They are all commercially available and can be used as received. For imidazole-based compounds, there is a lone pair of electrons at the N (3) position of the five membered ring. The carbon atom in CO_2 is an electron-deficient center, which can be used as an electrophile to react with nucleophilic reagents. This means a good affinity of CO_2 molecule to imidazole-based compounds. Furthermore, the vapor pressure of imidazole solid is extremely low (e.g., 0.008 mmHg for 2-ethyl-4-methylimidazole, Table S1). In contrast, the vapor pressure of MEA, a commonly used CO_2 absorbent in industry, is about 0.5 mmHg at 25 °C. A low vapor pressure limits the volitation of the absorbent and hence, is advantageous to reducing the loss of the absorbent in the process of CO_2 capture.

To perform the CO_2 capture, 1 g of the imidazole solid was dissolved in 14 g of DI water to obtain an aqueous solution. Next, CO_2 (purity 99.99%) was continuously input to the solution at a constant flow rate of 90 standard cubic centimeters per minute (SCCM). The weight change of the solution was measured every 2 min (Figure 1a–j). Table S2 shows the summary of CO_2 capture capacity of various imidazole aqueous solutions and compares them with the results obtained by Tomizaki et al. [31] and Evjen et al. [32] As shown in Figure S4, the molar CO_2 absorption capacity of the imidazoles were positively correlated with pK_a. Of the ten imidazole solids (Figure 1k), the aqueous solution of 2-ethyl-4-methylimidazole displayed the shortest saturation time (ca. 8 min) and the maximum molar absorption capacity of 0.88 $mol_{CO_2} \cdot mol^{-1}{}_{imidazole}$ ($mol \cdot mol^{-1}$ for clarity). The short saturation absorption time demonstrates that the aqueous solution of 2-ethyl-4-methylimidazole enables a favorable absorption kinetics in CO_2 capture. The molar absorption capacity of 0.88 mol/mol indicates that approximately one molecule of 2-ethyl-4-methylimidazole interacts with one molecule of CO_2. For the commonly used amine system, it usually needs two molecules of amine to capture of one molecule of CO_2 to form carbamate. Consequently, 2-ethyl-4-methylimidazole shows a nearly 1:1 molecular utilization in the CO_2 capture besides the favorable absorption kinetics. It should be noted that water in our system is a critical component in the promotion of the capture performance of 2-ethyl-4-methylimidazole. In the control experiments (Figure S5), there is no absorption of CO_2 when anhydrous solid of 2-ethyl-4-methylimidazole was used alone. The phenomenon is attributable to the interaction between 2-ethyl-4-methylimidazole and water. There is a lone electron pair on the N (3) of the imidazole ring, and this alkaline site

can combine with H^+ in H_2O to promote the ionization of water [48], thus producing OH^- ions to absorb CO_2.

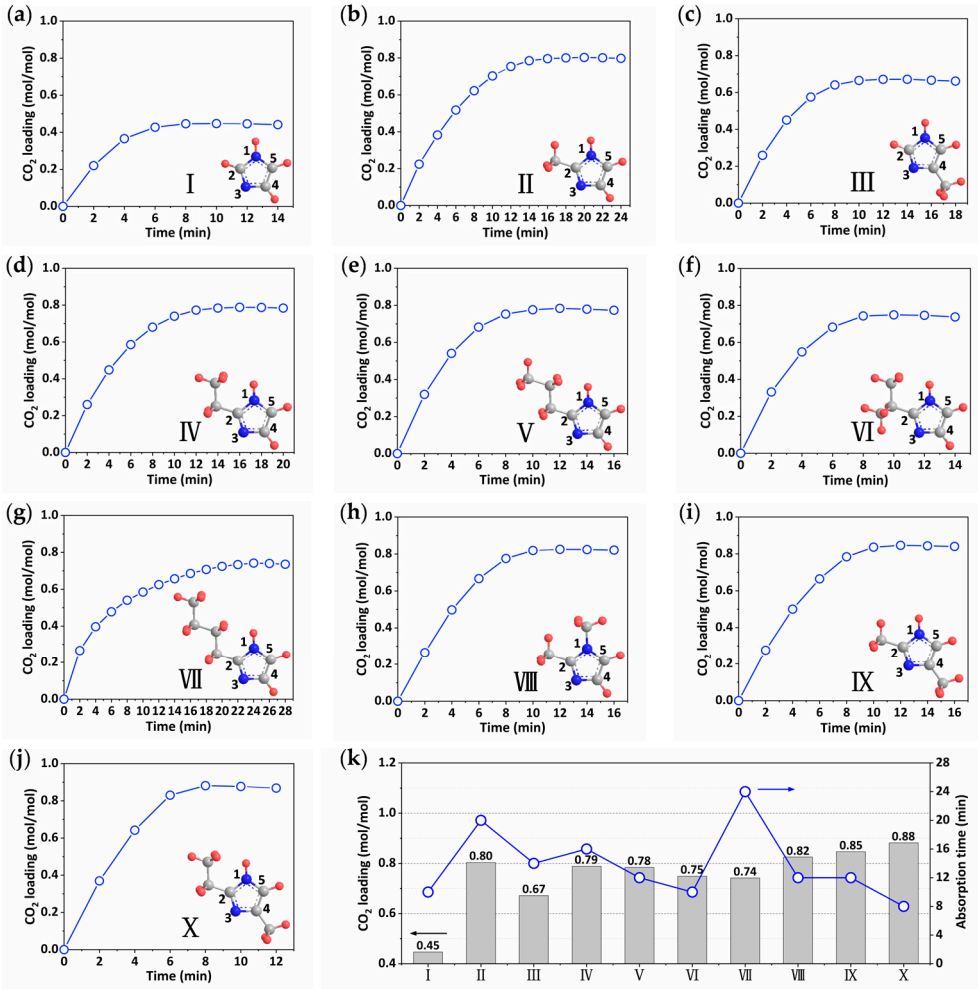

Figure 1. Studies of CO_2 capture over ten different imidazole solids. (**a**) Imidazole, (**b**) 2-methylimidazole, (**c**) 4-methylimidazole, (**d**) 2-ethylimidazole, (**e**) 2-propylimidazole, (**f**) 2-isopropylimidazole, (**g**) 2-buthylimidazole, (**h**) 1,2-dimethylimidazole, (**i**) 2,4-dimethylimidazole, and (**j**) 2-ethyl-4-methylimidazole. (**k**) Comparisons of CO_2 absorption capacity and absorption time of the ten imidazole solids.

The interactions of the aqueous solution of 2-ethyl-4-methylimidazole with nitrogen (N_2) and oxygen (O_2) were studied too, for the purpose of gaining insight into the selectivity of the system. As seen from Figure S6, the pressure of the flask containing the solution could remain unchanged over one week in the presence of N_2 and O_2. Under identical condition, the pressure of the flask filled by CO_2 was negative after stirring for 3 min, attributable to the absorption of CO_2 by the solution. The comparison demonstrates that the aqueous solution of 2-ethyl-4-methylimidazole has a good CO_2 selectivity, which means that it is capable of separating CO_2 from industrial flue gases and even ambient air, as will be shown later.

Next, the mass ratio of 2-ethyl-4-methylimidazole to water was adjusted to be 0.5:14.5, 2:13, and 3:12 (total mass of the system keeping at 15 g), and the CO_2 absorption performance of the system under different mass fraction was studied (Figure 2a). For the solution with a mass ratio of 0.5:14.5, the CO_2 saturation absorption time is 6 min. With the increase in the percentage of 2-ethyl-4-methylimidazole in the solution, the saturation absorption time is prolonged, which is around 8, 16, and 26 min corresponding to the system with a mass ratio 1:14, 2:13, and 3:12, respectively. Moreover, it can be seen that

a low mass fraction of 2-ethyl-4-methylimidazole is advantageous to achieving a high molar absorption capacity. For the 0.5:14.5 system, the molar absorption capacity can reach 1.01 mol·mol^{-1}, indicative of a 100% utilization of the 2-ethyl-4-methylimidazole molecule. For the 3:12 system, the molar absorption capacity decreases to 0.69 mol·mol^{-1}. On the basis of the saturation absorption capacity and the time, an average CO_2 absorption rates were calculated to be 0.17, 0.11, 0.05, and 0.03 mol·mol^{-1}·min^{-1} for the system with a mass fraction of 0.5:14.5, 1:14, 2:13, and 3:12, respectively (Figure 2b). Figure S7 shows the CO_2 capture capacity of 2-ethyl-4-methylimidazole solutions with different mass fractions. It can be seen that the CO_2 capacity of pure water is only 0.024 g, which can be improved by adding 2-ethyl-4-methylimidazole, and it has the CO_2 capacity of 0.821 g when the ratio is 3:12. Moreover, one may observe a slight decline of the molar absorption capacity in the 0.5:14.5 and 1:14 systems after the saturation absorption (Figure 2a). It is attributed to the removal of the moisture by the continuous CO_2 flow, thus leading to a reduction of the mass of the system. However, in the systems with a mass fraction of 2:13 and 3:12, the loss of the moisture is avoided and the systems are quite stable.

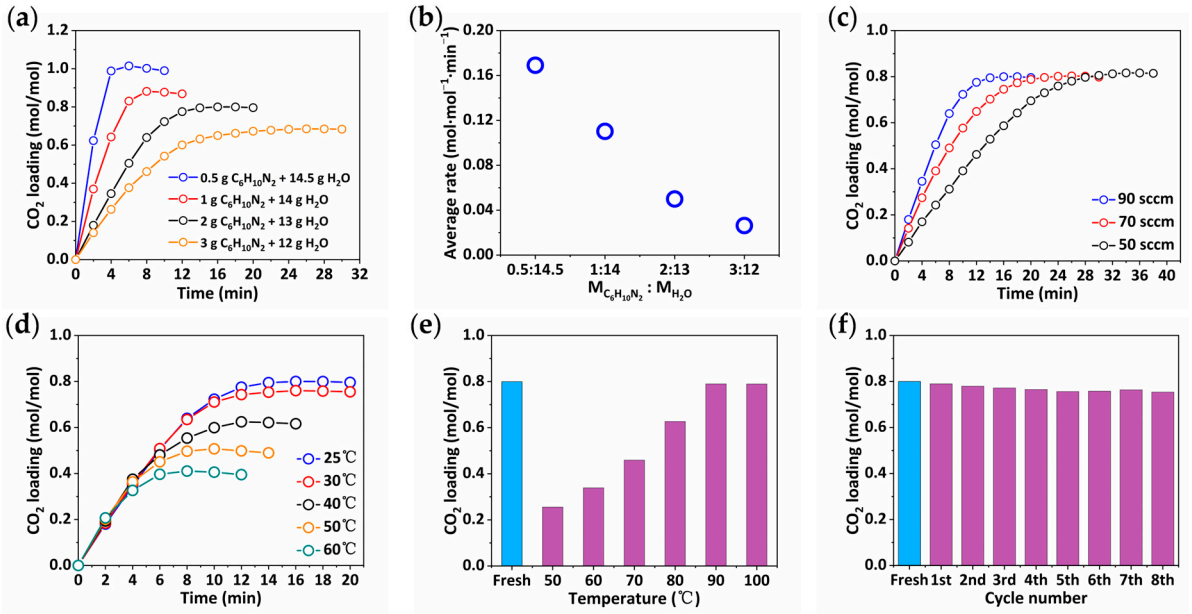

Figure 2. CO_2 absorption–desorption performance of 2-ethyl-4-methylimidazole. (**a**) CO_2 absorption curves of the 2-ethyl-4-methylimidazole solution with a mass fraction of 0.5:14.5, 1:14, 2:13, and 3:12 (CO_2 flow rate 90 SCCM). (**b**) Average molar absorption rates of the four 2-ethyl-4-methylimidazole solutions. (**c**) CO_2 absorption curves of the 2:13 system at different gas flow rates. (**d**) CO_2 absorption curves of the 2:13 system at different temperatures. (**e**) CO_2 desorption capacity of the 2:13 system at different temperatures. (**f**) Cycle stability of the 2:13 system (desorption temperature 90 °C).

The different CO_2 capture performances of the 2-ethyl-4-methylimidazole solutions with a mass fraction of 0.5:14.5, 1:14, 2:13, and 3:12 are related to the viscosity of the system. As shown in Figure S8, the viscosity of the solution is increased with the increase in the proportion of 2-ethyl-4-methylimidazole. High viscosity is disadvantageous to the mass transfer efficiency as well as heat exchange efficiency, thus weakening the interaction of the absorbent with CO_2. As a result, the aqueous solution with the lowest proportion of 2-ethyl-4-methylimidazole shows the largest molar absorption capacity and highest rate. On the other hand, a high viscosity prevents the volatilization of the moisture. Consequently, the 2:13 and 3:12 systems could display a better stability. Considering that the solution with the mass fraction of 2:13 has good stability and appropriate absorption capacity, we focus on this system in the subsequent studies.

Figure 2c shows the CO_2 absorption curve of the 2:13 system at different CO_2 flow rates. It can be seen that, with the increase in the flow rate, CO_2 absorption rate is speed up

and the absorption saturation time is shortened. Based on the gas absorption double-film theory, the resistance of the gas absorption process is mainly concentrated in the gas film and liquid film. Increasing the gas flow rate can reduce the thickness of the gas film layer at the interface, thus reducing the gas phase mass transfer resistance and effectively improving the absorption rate. However, the increase in gas flow rate will make the contact time between gas molecules and adsorbent too short, which is not conducive to gas adsorption. Herein, when the gas flow rate increases from 50 SCCM to 90 SCCM, the CO_2 absorption capacity slightly decreases from 0.82 mol/mol to 0.80 mol·mol^{-1}. Therefore, the gas flow rate should be reasonably selected based on absorption time, absorption capacity, and other factors to improve absorption efficiency [49]. In this study, the gas flow rate is controlled at 90 SCCM because of the relatively short saturation absorption time.

Temperature plays a key role in the performance of the absorbent as it affects the evaporation of the absorbent and the solubility of CO_2 [50,51]. Figure 2d shows the absorption behavior of the 3:12 system at 25, 30, 40, 50, and 60 °C. The results reveal that the saturation absorption time is inversely proportional to the temperature. At high temperature, the average kinetic energy of gas molecules increases, which accelerates the diffusion of CO_2 and improves the interactions of CO_2 with the absorbent. But high temperature decreases the solubility of CO_2 and facilitates the desorption of CO_2 as the desorption reaction is endothermic. This leads to a declined absorption capacity of CO_2 at the high temperature (e.g., 0.41 mol·mol^{-1} at 60 °C versus 0.76 mol·mol^{-1} at 30 °C). Consequently, CO_2 capture is performed at 25 °C (room temperature) because this temperature allows a high absorption capacity and does not require additional energy input.

In order to reduce the environmental pollution and investment costs, CO_2 absorbent needs to be recycled for many times. For commercial applications, they should be stable in the long adsorption–desorption cycle [52]. Desorption heat is the energy required for the decomposition of substances (such as bicarbonate and carbonate) formed in the reaction process, and is also the main source of energy required for the regeneration of the loaded CO_2 solution [53]. Therefore, desorption performance is an important index to evaluate the adsorbent. Figure 2e shows the desorption behavior of the 2:13 system in the temperature range of 50~100 °C. Prior to the desorption experiments, the system was interacted with CO_2 at 25 °C to reach the saturation absorption capacity (0.80 mol·mol^{-1}, indicated by blue column in Figure 2e). When the desorption temperatures of 90 and 100 °C were employed, almost all absorbed CO_2 can be released by the system (namely a 100% desorption efficiency). With the decrease in the temperature, the desorption efficiency was declined. At 50 °C, only 31.9% of CO_2 was released by the system. This is because the desorption process of CO_2 is an endothermic reaction. The higher the temperature, the higher the desorption efficiency and the more CO_2 can be released. It is worth noting that the desorption temperature is relatively low herein. To efficiently regenerate CO_2 from amine-based systems, a high desorption temperature (>100 °C) is usually involved (Table S3) [51,54–63]. Figure 2f shows the absorption–desorption cycle results of the 2:13 system. After the eight cycles, the system only loses 5.8% of its initial absorption capacity, suggesting that the aqueous 2-ethyl-4-methylimidazole solution for CO_2 capture is cyclable and stable. MEA is known to be widely used in the industry as a CO_2 absorbent. For a comparison, we studied the CO_2 absorption–desorption performances of MEA under the condition identical to that of 2-ethyl-4-methylimidazole solution. As shown in Figure S9a, the saturation absorption capacity is 0.83 mol·mol^{-1}, close to the value for 2-ethyl-4-methylimidazole solution. However, the absorption capacity was decreased by 84% in the second cycle (Figure S9b). The control experiment highlights the superiority of 2-ethyl-4-methylimidazole solution for CO_2 capture.

To understand the absorption–desorption mechanism of CO_2 in the aqueous solution of 2-ethyl-4-methylimidazole, time-related *in-situ* attenuated total reflection infrared (ATR-IR) absorption spectroscopy and ^{13}C NMR spectroscopy measurements were carried out. The ATR-IR spectrometer equips with a liquid-nitrogen-cooled mercury cadmium telluride (MCT) detector and a plug-in optical fiber probe, which enable to acquire the IR

spectrum in real time (Figure 3a,b). In the process of CO_2 absorption, three IR bands locating at 1010, 1357, and 2341 cm^{-1} were developed and their intensities were increased with the prolongation of CO_2 absorption time (Figure 3c–e). The band of 1010 cm^{-1} (Figure 3c) is assigned to the C-OH stretching vibration of the bicarbonate. The band of 1357 cm^{-1} (Figure 3d) is assigned to the COO^- symmetric stretching vibration of the bicarbonate. As for the band of 2341 cm^{-1} (Figure 3e), it is attributed to the asymmetric stretching vibration of CO_2. In situ IR results clearly demonstrate that the aqueous solution of 2-ethyl-4-methylimidazole is capable of capturing CO_2. Simultaneously, the IR data indicate that CO_2 is transformed to HCO_3^- in the system. The detailed mechanism of CO_2 capture by the system is discussed later. When the system is heated in a constant temperature water bath (90 °C), the three IR bands are weakened and ultimately disappeared (Figure 3f–h), indicating that CO_2 could be released thoroughly by the system. According to gas chromatography and mass spectrometry measurements (Figure S10), the released gas is pure CO_2. No other gaseous products were detected.

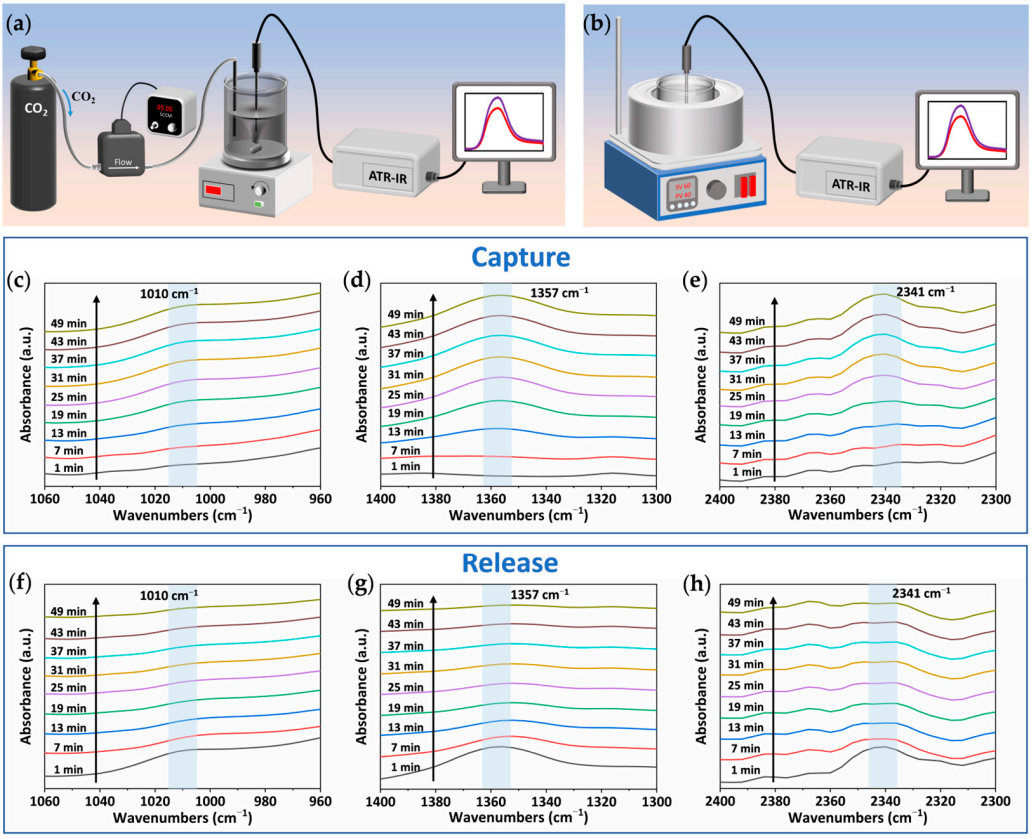

Figure 3. In situ ATR-IR spectra of CO_2 absorption–desorption process. (**a**) Schematic of in situ ATR-IR CO_2 absorption setup. (**b**) Schematic of in situ ATR-IR CO_2 desorption setup. (**c**–**e**) In situ ATR-IR absorption CO_2 spectra of 2-ethyl-4-methylimidazole. (**f**–**h**) In situ ATR-IR desorption CO_2 spectra of 2-ethyl-4-methylimidazole.

Figure 4 shows the ^{13}C NMR spectroscopy study of the absorption and desorption of CO_2 in the aqueous solution of 2-ethyl-4-methylimidazole. During the absorption of CO_2, bicarbonate ions at 160 ppm were produced (Figure 4a), consistent with the afore-mentioned IR data. Standard ^{13}C NMR spectra of sodium carbonate and sodium bicarbonate were shown in Figure S7 for comparisons. Based on the IR and NMR results, a water-assisted CO_2 capture mechanism is proposed and shown in Figure 4b. 2-Ethyl-4-methylimidazole first combines with the hydrogen ion in the solution, inducing the water molecules to ionize continuously. Thus, OH^- ions are produced and react with CO_2 to yield HCO_3^-. As the reaction proceeds, the pH value of the solution decreases, the conductivity increases

(Figure S12), and the HCO_3^- signal gradually increases, indicating that bicarbonate ions are accumulated in the process of the absorption of CO_2. When the system loaded by CO_2 is heated, the signal of the bicarbonate peak at 160 ppm gradually weakens and finally disappears owing to the thermal release of CO_2 (Figure 4c). In the process of CO_2 desorption, bicarbonate ions act as proton receptors to help the deprotonation of protonated imidazole (Figure 4d). H_2O molecules are also underlying proton receptors in the system. However, HCO_3^- ion is a stronger base than H_2O, and protons are preferred to bind with the former to form carbonic acid (H_2CO_3) rather than H_3O^+. H_2CO_3 is an unstable molecule, which is every easy to decompose into CO_2 upon heating. Moreover, the mechanism studies clarify the reason why our system is easier to release CO_2 in comparison to the amine systems (Table S3) [51,54–63]. In the amine systems, carbamates are the intermediates in the process of CO_2 absorption and desorption. In our system, HCO_3^- and H_2CO_3 serve as the intermediates, which are known to decompose at low temperatures. Consequently, the formation of HCO_3^- and H_2CO_3 can reduce the heat load in the process of regenerating the 2-ethyl-4-methylimidazole solution. Whereas the decomposition of carbamate intermediates is relatively difficult and hence, a larger heat load is required for the regeneration of the amine systems [59,64,65].

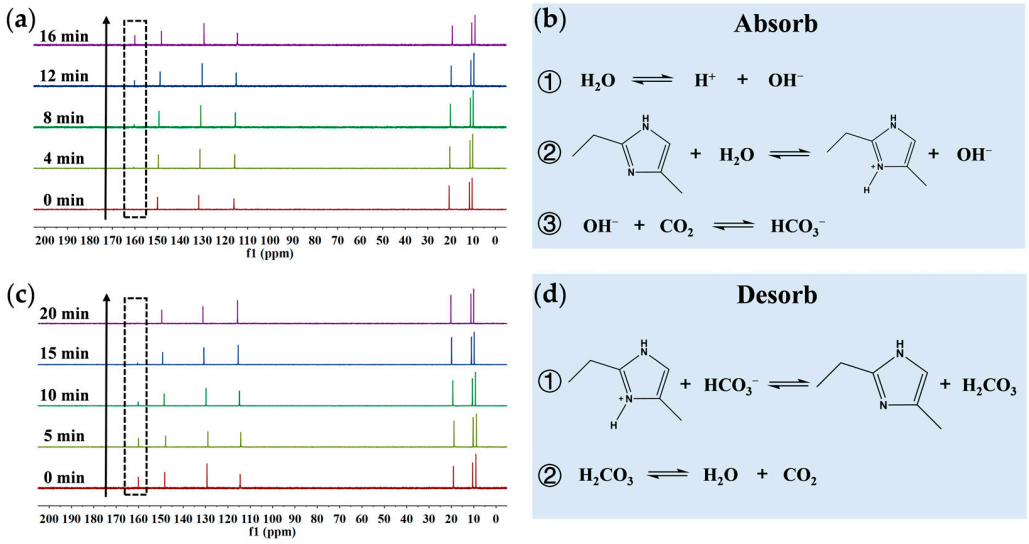

Figure 4. Mechanism of absorption–desorption of CO_2. (**a**) Changes in ^{13}C NMR spectra of 2-ethyl-4-methylimidazole during CO_2 absorption. (**b**) Mechanism of CO_2 absorption by 2-ethyl-4-methylimidazole. (**c**) Changes in ^{13}C NMR spectra of 2-ethyl-4-methylimidazole during CO_2 desorption. (**d**) Mechanism of CO_2 desorption by 2-ethyl-4-methylimidazole.

From the perspective of practical implementation, CO_2 capture usually deals with CO_2 emissions from point sources such as power stations, refineries, cement plants, steel industrial facilities, and so on, where the concentration of CO_2 is relatively low (volume fraction 10%~20%). When the synthetic flue gas was passed through the aqueous solution of 2-ethyl-4-methylimidazole at a flow rate of 50 SCCM at room temperature, a saturation absorption of CO_2 needs 192 min and the molar absorption capacity is 0.56 mol·mol^{-1} (Figure 5a). When the gas flow rate is increased to 90 SCCM, the absorption time is relatively short (124 min) and the molar absorption capacity is 0.54 mol/mol. In comparison to the capture of pure CO_2 (Figure 2c), the absorption rate and absorption capacity of 15% CO_2 by the 2-ethyl-4-methylimidazole solution are both decreased. The results are understandable because the low CO_2 partial pressure in the synthetic flue gas reduces the gas phase driving force and distribution coefficient in the liquid phase, thus leading to a varied performance of the system. Figure 5b shows the cycle capacity of 2-ethyl-4-methylimidazole solution toward the synthetic flue gas at the desorption temperature of 90 °C. It can be seen that under the conditions of low partial pressure of CO_2 and the presence of O_2, the 2-ethyl-4-

methylimidazole solution still display a good stability and cyclability. After eight cycles, the molar absorption capacity is only decreased by 7.1%, slightly higher than the value of 5.8% for pure CO_2 feed. The ^{13}C NMR spectrum shows that the bicarbonate ion is generated during CO_2 absorption and disappears during desorption (Figure S13a), suggesting a capture mechanism same as that for pure CO_2 (Figure 4a). After eight cycles, no other species were detected by ^{13}C NMR spectroscopy except for 2-ethyl-4-methylimidazole in the solution (Figure S13b).

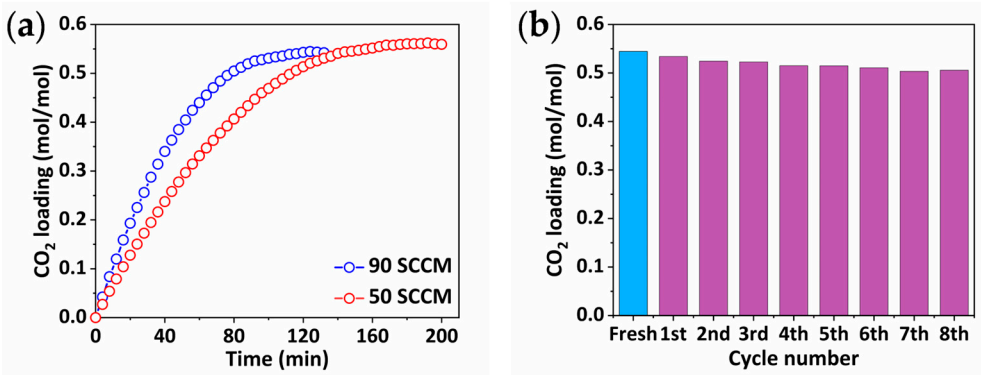

Figure 5. The capture of CO_2 in flue gas by 2-ethyl-4-methylimidazole solution. (**a**) CO_2 absorption curves of the 2-ethyl-4-methylimidazole solution at different gas flow rates. (**b**) Cycle stability of the 2-ethyl-4-methylimidazole solution (desorption temperature 90 °C).

Furthermore, the performance of 2-ethyl-4-methylimidazole solution for CO_2 separation from flue gas was studied using the bubble absorption setup (Figure 6a). At the initial stage (0~100 min), CO_2 in the flue gas can be captured completely by the setup (Figure 6b). After that, the concentration of CO_2 in the offgas is increased gradually and reached a platform at about 500 min (absorption saturation). Through desorption, the purified CO_2 can be transfer to the steel cylinder with the assistance of the compressor (Figure 6c,d). By repeating the above process, low-cost CO_2 capture and storage can be realized.

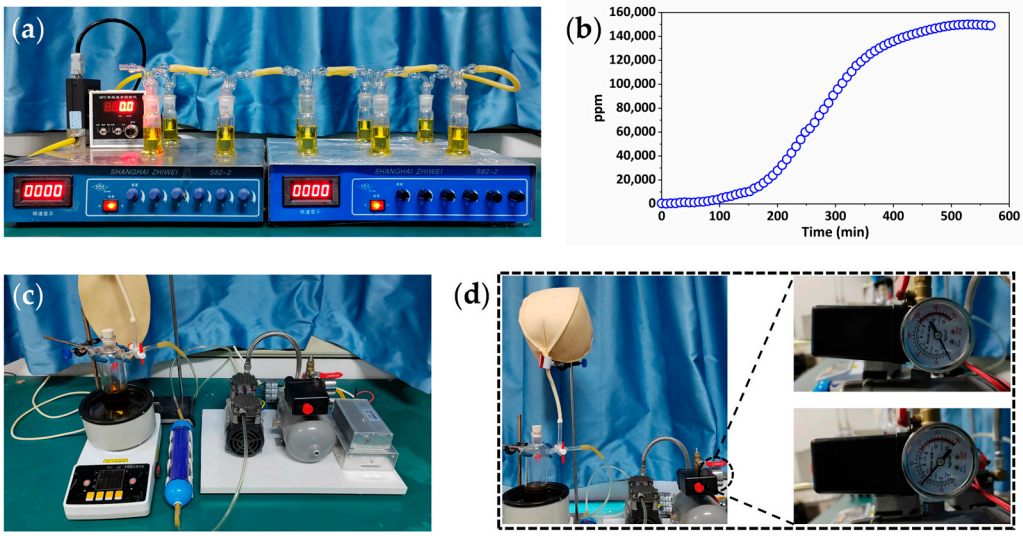

Figure 6. 2-Ethyl-4-methylimidazole solution for separation and purification of CO_2 from flue gas. (**a**) Photograph of bubbling absorption setup. (**b**) Absorption curve of CO_2 capture from flue gas by bubble absorption setup (gas flow rate: 90 SCCM). (**c**) Photograph of desorption setup. (**d**) Photographs showing that the released CO_2 can be compressed by an air compressor and stored in a steel cylinder.

In addition to the capture of CO_2 from large fixed-point sources, a closed carbon cycle also needs to deal with scattered emissions from small emitters. Compared with point source capture, capturing CO_2 from dilution sources presents greater challenges. Herein we studied the direct capture of CO_2 from the air by the aqueous solution of 2-ethyl-4-methylimidazole (2 g of 2-ethyl-4-methylimidazole dissolved in 13 g of water). After exposure to air for certain hours, concentrated CO_2 was collected by heating the 2-ethyl-4-methylimidazole solution. It can be seen from Figure S14a,b, for an exposure time of 12 h, the concentration of CO_2 is about 8000 ppm, 20 folds of that of environmental CO_2. With the extension of the exposure time, CO_2 can be further concentrated and enriched and its reaches around 40,000 ppm after 72 h, which has increased by 100 folds relative to that of the environmental CO_2.

4. Conclusions

In conclusion, a series of low molecular weight imidazole solids were demonstrated as the absorbent for CO_2 capture. Among them, the aqueous solution of 2-ethyl-4-methylimidazole is found to show excellent CO_2 capture performance. The solution displays a maximum molar absorption capacity of 1.0 mol·mol^{-1} at the mass ratio 0.5 g 2-ethyl-4-methylimidazole to 14.5 g water, demonstrating that one molecule of 2-ethyl-4-methylimidazole can capture one molecule of CO_2, and all absorbed CO_2 is able to be released upon heating the 2-ethyl-4-methylimidazole solution at 90 °C. After eight absorption–desorption cycles, the reduced molar absorption capacity of the system is less than 10%, suggesting a good stability. Mechanism studies reveal that HCO_3^- and H_2CO_3 serve as the intermediates in the process of CO_2 absorption and desorption. Moreover, the aqueous solution of 2-ethyl-4-methylimidazole is capable of efficiently separating and purifying CO_2 from flue gas and even ambient air. Therefore, aqueous solution of 2-ethyl-4-methylimidazole is a promising low-cost CO_2 absorbent for practical implementation.

Supplementary Materials: The following supporting information can be downloaded at: https://www.mdpi.com/article/10.3390/separations10040236/s1. Figure S1: Schematic of experimental setups. (a) CO_2 absorption setup. (b) CO_2 desorption setup. Figure S2: (a) Schematic of the bubbling absorption setup, which consists of 10 bubbling reactors connected in series. (b) Schematic of desorption and compression setup. Figure S3: Schematic of imidazole aqueous solution direct air capture and heat concentration of CO_2. Figure S4: Relationship between molar absorption of CO_2 and p*K*a. Figure S5: Study on CO_2 absorption capacity of 2-ethyl-4-methylimidazole by using anhydrous solid and aqueous solution. (a) Photographs showing the absorption of CO_2 by pure 2-ethyl-4-methylimidazole solid. (b) Photographs showing the absorption of CO_2 by 2-ethyl-4-methylimidazole aqueous solution. Figure S6: Study on selective gas absorption. (a) Photograph of reaction experiment setup. (b–d) Photographs showing that the reading of the pressure gauge pointer changes under different gas feeds. (b) N_2, (c) O_2, (d) CO_2. Figure S7: CO_2 absorption capacity of 2-ethyl-4-methylimidazole solution with different mass fractions. Figure S8: (a) Photograph of 2-ethyl-4-methylimidazole solution with different mass fractions. (b) Viscosities of various 2-ethyl-4-methylimidazole solutions. Figure S9: CO_2 absorption–desorption performance of ethanolamine. (a) Absorption capacity curve of ethanolamine with time (2 g MEA + 13 mL H_2O). (b) After desorption at 90 °C, the secondary reabsorption rate of MEA significantly decreases. Figure S10: (a) Gas chromatography measurements of heat released gas. (b) Mass spectrum of heat released gas. Figure S11: (a) ^{13}C NMR spectrum of $NaHCO_3$ aqueous solution. (b) ^{13}C NMR spectrum of $NaCO_3$ aqueous solution. Figure S12: Changes in pH value and conductivity with time during CO_2 absorption by 2-ethyl-4-methylimidazole aqueous solution. (a) pH change. (b) Conductivity change. Figure S13: (a) ^{13}C NMR spectra of 2-ethyl-4-methylimidazole during absorption–desorption of CO_2 from the synthetic flue gas. (b) ^{13}C NMR spectrum of 2-ethyl-4-methylimidazole after 8 cycles. Figure S14: The capture of ambient air by 2-ethyl-4-methylimidazole. (a) Curve of CO_2 enrichment concentration with capture time. (b) Corresponds to the change of peak area detected by gas chromatography. Table S1: Basic properties of ten solid imidazoles. Table S2: Summary of CO_2 capture capacity of various imidazole aqueous solutions. Table S3: Comparison of 2-ethyl-4-methylimidazole and amine absorbents.

Author Contributions: Conceptualization, methodology, X.Z. and X.C.; validation, J.W. and X.L.; formal analysis, X.L.; investigation, J.W.; data curation, X.Z.; writing—original draft preparation, X.Z.; writing—review and editing, Y.Y. and X.C.; visualization, X.Z. and L.G.; supervision, Y.Y. and L.G.; project administration, X.C.; funding acquisition, X.C. All authors have read and agreed to the published version of the manuscript.

Funding: This work is supported by the National Natural Science Foundation of China (Nos. 22275074).

Data Availability Statement: Not applicable.

Acknowledgments: The authors thank the support of the National Natural Science Foundation of China.

Conflicts of Interest: The authors declare no conflict of interest.

References

1. Hofmann, D.J.; Butler, J.H.; Tans, P.P. A new look at atmospheric carbon dioxide. *Atmos. Environ.* **2009**, *43*, 2084–2086. [CrossRef]
2. Sanz-Pérez, E.S.; Murdock, C.R.; Didas, S.A.; Jones, C.W. Direct Capture of CO_2 from Ambient Air. *Chem. Rev.* **2016**, *116*, 11840–11876. [CrossRef] [PubMed]
3. Kontos, G.; Soldatou, M.A.; Tzimpilis, E.; Tsivintzelis, I. Solubility of CO_2 in 2-Amino-2-methyl-1-propanol (AMP) and 3-(Methylamino)propylamine (MAPA): Experimental Investigation and Modeling with the Cubic-Plus-Association and the Modified Kent-Eisenberg Models. *Separations* **2022**, *9*, 338–358. [CrossRef]
4. Samset, B.H.; Fuglestvedt, J.S.; Lund, M.T. Delayed emergence of a global temperature response after emission mitigation. *Nat. Commun.* **2020**, *11*, 3261–3270. [CrossRef] [PubMed]
5. Pauw, P.; Mbeva, K.; van Asselt, H. Subtle differentiation of countries' responsibilities under the Paris Agreement. *Palgrave Commun.* **2019**, *5*, 86–92. [CrossRef]
6. Wei, Y.M.; Han, R.; Wang, C.; Yu, B.; Liang, Q.M.; Yuan, X.C.; Chang, J.; Zhao, Q.; Liao, H.; Tang, B.; et al. Self-preservation strategy for approaching global warming targets in the post-Paris Agreement era. *Nat. Commun.* **2020**, *11*, 1624–1636. [CrossRef]
7. Bui, M.; Adjiman, C.S.; Bardow, A.; Anthony, E.J.; Boston, A.; Brown, S.; Fennell, P.S.; Fuss, S.; Galindo, A.; Hackett, L.A.; et al. Carbon capture and storage (CCS): The way forward. *Energy Envrion. Sci.* **2018**, *11*, 1062–1176. [CrossRef]
8. Paltsev, S.; Morris, J.; Kheshgi, H.; Herzog, H. Hard-to-Abate Sectors: The role of industrial carbon capture and storage (CCS) in emission mitigation. *Appl. Energy* **2021**, *300*, 117322–117332. [CrossRef]
9. Sebastiani, F.; Lucking, L.; Sarić, M.; James, J.; Boon, J.; van Dijk, H.J.A.E.; Cobden, P.; Pieterse, J.A.Z. Steam and Pressure Management for the Conversion of Steelworks Arising Gases to H_2 with CO_2 Capture by Stepwise Technology. *Separations* **2022**, *9*, 20–40. [CrossRef]
10. Mac Dowell, N.; Fennell, P.S.; Shah, N.; Maitland, G.C. The role of CO_2 capture and utilization in mitigating climate change. *Nat. Clim. Chang.* **2017**, *7*, 243–249. [CrossRef]
11. Jones, W.D. Carbon Capture and Conversion. *J. Am. Chem. Soc.* **2020**, *142*, 4955–4957. [CrossRef]
12. Sullivan, I.; Goryachev, A.; Digdaya, I.A.; Li, X.; Atwater, H.A.; Vermaas, D.A.; Xiang, C. Coupling electrochemical CO_2 conversion with CO_2 capture. *Nat. Catal.* **2021**, *4*, 952–958. [CrossRef]
13. Gao, W.; Liang, S.; Wang, R.; Jiang, Q.; Zhang, Y.; Zheng, Q.; Xie, B.; Toe, C.Y.; Zhu, X.; Wang, J.; et al. Industrial carbon dioxide capture and utilization: State of the art and future challenges. *Chem. Soc. Rev.* **2020**, *49*, 8584–8686. [CrossRef]
14. Reynolds, A.J.; Verheyen, T.V.; Adeloju, S.B.; Meuleman, E.; Feron, P. Towards Commercial Scale Postcombustion Capture of CO_2 with Monoethanolamine Solvent: Key Considerations for Solvent Management and Environmental Impacts. *Environ. Sci. Technol.* **2012**, *46*, 3643–3654. [CrossRef]
15. Hwang, G.S.; Stowe, H.M.; Paek, E.; Manogaran, D. Reaction mechanisms of aqueous monoethanolamine with carbon dioxide: A combined quantum chemical and molecular dynamics study. *Phys. Chem. Chem. Phys.* **2015**, *17*, 831–839. [CrossRef]
16. Corrêa, L.F.F.; Thomsen, K.; Jayaweera, I.; Jayaweera, P.; Fosbøl, P.L. Vapor−Liquid Equilibrium Measurements for Aqueous Mixtures of NH_3 + MDEA + CO_2 and KOH + MDEA. *J. Chem. Eng. Data* **2022**, *67*, 3443–3456. [CrossRef]
17. Dashti, A.; Raji, M.; Razmi, A.; Rezaei, N.; Zendehboudi, S.; Asghari, M. Efficient hybrid modeling of CO_2 absorption in aqueous solution of piperazine: Applications to energy and environment. *Chem. Eng. Res. Des.* **2019**, *144*, 405–417. [CrossRef]
18. Wei, K.; Guan, H.; Luo, Q.; He, J.; Sun, S. Recent advances in CO_2 capture and reduction. *Nanoscale* **2022**, *14*, 11869–11891. [CrossRef] [PubMed]
19. Liu, S.; Gao, H.; He, C.; Liang, Z. Experimental evaluation of highly efficient primary and secondary amines with lower energy by a novel method for post-combustion CO_2 capture. *Appl. Energy* **2019**, *233–234*, 443–452. [CrossRef]
20. Singto, S.; Supap, T.; Idem, R.; Tontiwachwuthikul, P.; Tantayanon, S.; Al-Marri, M.J.; Benamor, A. Synthesis of new amines for enhanced carbon dioxide (CO_2) capture performance: The effect of chemical structure on equilibrium solubility, cyclic capacity, kinetics of absorption and regeneration, and heats of absorption and regeneration. *Sep. Purif. Technol.* **2016**, *167*, 97–107. [CrossRef]
21. Luo, X.; Liu, S.; Gao, H.; Liao, H.; Tontiwachwuthikul, P.; Liang, Z. An improved fast screening method for single and blended amine-based solvents for post-combustion CO_2 capture. *Sep. Purif. Technol.* **2016**, *169*, 279–288. [CrossRef]

22. Zhang, X.; Zhang, X.; Liu, H.; Li, W.; Xiao, M.; Gao, H.; Liang, Z. Reduction of energy requirement of CO_2 desorption from a rich CO_2-loaded MEA solution by using solid acid catalysts. *Appl. Energy* **2017**, *202*, 673–684. [CrossRef]
23. Alivand, M.S.; Mazaheri, O.; Wu, Y.; Zavabeti, A.; Stevens, G.W.; Scholes, C.A.; Mumford, K.A. Water-Dispersible Nanocatalysts with Engineered Structures: The New Generation of Nanomaterials for Energy-Efficient CO_2 Capture. *ACS Appl. Mater. Interfaces* **2021**, *13*, 57294–57305. [CrossRef]
24. Alivand, M.S.; Mazaheri, O.; Wu, Y.; Zavabeti, A.; Christofferson, A.J.; Meftahi, N.; Russo, S.P.; Stevens, G.W.; Scholes, C.A.; Mumford, K.A. Engineered assembly of water-dispersible nanocatalysts enables low-cost and green CO_2 capture. *Nat. Commun.* **2022**, *13*, 1249–1259. [CrossRef]
25. Srikanth, C.S.; Chuang, S.S.C. Infrared Study of Strongly and Weakly Adsorbed CO_2 on Fresh and Oxidatively Degraded Amine Sorbents. *J. Phys. Chem. C* **2013**, *117*, 9196–9205. [CrossRef]
26. Pang, S.H.; Lee, L.C.; Sakwa-Novak, M.A.; Lively, R.P.; Jones, C.W. Design of Aminopolymer Structure to Enhance Performance and Stability of CO_2 Sorbents: Poly(propylenimine) vs Poly(ethylenimine). *J. Am. Chem. Soc.* **2017**, *139*, 3627–3630. [CrossRef] [PubMed]
27. Li, W.; Bollini, P.; Didas, S.A.; Choi, S.; Drese, J.H.; Jones, C.W. Structural changes of silica mesocellular foam supported amine-functionalized CO_2 adsorbents upon exposure to steam. *ACS Appl. Mater. Interfaces* **2010**, *2*, 3363–3372. [CrossRef] [PubMed]
28. Ahmadalinezhad, A.; Sayari, A. Oxidative degradation of silica-supported polyethylenimine for CO_2 adsorption: Insights into the nature of deactivated species. *Phys. Chem. Chem. Phys.* **2014**, *16*, 1529–1535. [CrossRef]
29. Longeras, O.; Gautier, A.; Ballerat-Busserolles, K.; Andanson, J.M. Tuning critical solution temperature for CO_2 capture by aqueous solution of amine. *J. Mol. Liq.* **2021**, *343*, 117628–117635. [CrossRef]
30. Zhang, L.; Peng, X.M.; Damu, G.L.; Geng, R.X.; Zhou, C.H. Comprehensive review in current developments of imidazole-based medicinal chemistry. *Med. Res. Rev.* **2014**, *34*, 340–437. [CrossRef] [PubMed]
31. Tomizaki, K.; Shimizu, S.; Onoda, M.; Fujioka, Y. Heats of Reaction and Vapor-Liquid Equilibria of Novel Chemical Absorbents for Absorption/Recovery of Pressurized Carbon Dioxide in Integrated Coal Gasification Combined Cycle-Carbon Capture and Storage Process. *Ind. Eng. Chem. Res.* **2010**, *49*, 1214–1221. [CrossRef]
32. Evjen, S.; Fiksdahl, A.; Pinto, D.D.D.; Knuutila, H.K. New polyalkylated imidazoles tailored for carbon dioxide capture. *Int. J. Greenh. Gas Control.* **2018**, *76*, 167–174. [CrossRef]
33. Shannon, M.S.; Bara, J.E. Properties of Alkylimidazoles as Solvents for CO_2 Capture and Comparisons to Imidazolium-Based Ionic Liquids. *Ind. Eng. Chem. Res.* **2011**, *50*, 8665–8677. [CrossRef]
34. Chen, W.; Huang, Z.; Liang, X.; Kontogeorgis, G.M.; Liu, B.; Chen, G. Experimental data and modeling of the CO_2 solubility in 2-methylimidazole aqueous solution. *Fuel* **2023**, *331*, 125694–125704. [CrossRef]
35. Lin, C.; Stedronsky, E.R.; Regen, S.L. pKa-Dependent Facilitated Transport of CO_2 across Hyperthin Polyelectrolyte Multilayers. *ACS Appl. Mater. Interfaces* **2017**, *9*, 19525–19528. [CrossRef]
36. Yan, H.; Zhang, G.; Liu, J.; Li, G.; Wang, Y. Highly efficient CO_2 adsorption by imidazole and tetraethylenepentamine functional sorbents: Optimization and analysis using response surface methodology. *J. Environ. Chem. Eng.* **2021**, *9*, 105639–105648. [CrossRef]
37. Li, Q.; Gao, G.; Wang, R.; Zhang, S.; An, S.; Wang, L. Role of 1-methylimidazole in regulating the CO_2 capture performance of triethylenetetramine-based biphasic solvents. *Int. J. Greenh. Gas Control.* **2021**, *108*, 103330–103339. [CrossRef]
38. Foorginezhad, S.; Yu, G.; Ji, X. Reviewing and screening ionic liquids and deep eutectic solvents for effective CO_2 capture. *Front. Chem.* **2022**, *10*, 951951–951974. [CrossRef]
39. Cheng, J.; Wu, C.; Gao, W.; Li, H.; Ma, Y.; Liu, S.; Yang, D. CO_2 Absorption Mechanism by the Deep Eutectic Solvents Formed by Monoethanolamine-Based Protic Ionic Liquid and Ethylene Glycol. *Int. J. Mol. Sci.* **2022**, *23*, 1893–1899. [CrossRef]
40. Emel'yanenko, V.N.; Portnova, S.V.; Verevkin, S.P.; Skrzypczak, A.; Schubert, T. Building blocks for ionic liquids: Vapor pressures and vaporization enthalpies of 1-(n-alkyl)-imidazoles. *J. Chem. Thermodyn.* **2011**, *43*, 1500–1505. [CrossRef]
41. Shannon, M.S.; Tedstone, J.M.; Danielsen, S.P.O.; Bara, J.E. Evaluation of Alkylimidazoles as Physical Solvents for CO_2/CH_4 Separation. *Ind. Eng. Chem. Res.* **2011**, *51*, 515–522. [CrossRef]
42. Martin, S.; Lepaumier, H.; Picq, D.; Kittel, J.; de Bruin, T.; Faraj, A.; Carrette, P.-L. New Amines for CO_2 Capture. IV. Degradation, Corrosion, and Quantitative Structure Property Relationship Model. *Ind. Eng. Chem. Res.* **2012**, *51*, 6283–6289. [CrossRef]
43. Evjen, S.; Wanderley, R.; Fiksdahl, A.; Knuutila, H.K. Viscosity, Density, and Volatility of Binary Mixtures of Imidazole, 2-Methylimidazole, 2,4,5-Trimethylimidazole, and 1,2,4,5-Tetramethylimidazole with Water. *J. Chem. Eng. Data* **2019**, *64*, 507–516. [CrossRef]
44. Song, C.; Kitamura, Y.; Li, S. Optimization of a novel cryogenic CO_2 capture process by response surface methodology (RSM). *J. Taiwan Inst. of Chem. Eng.* **2014**, *45*, 1666–1676. [CrossRef]
45. Li, Y.; Gao, J.; Li, J.; Li, Y.; Bernards, M.T.; Tao, M.; He, Y.; Shi, Y. Screening and Performance Evaluation of Triethylenetetramine Nonaqueous Solutions for CO_2 Capture with Microwave Regeneration. *Energy Fuels* **2020**, *34*, 11270–11281. [CrossRef]
46. Qian, W.; Hao, J.; Zhu, M.; Sun, P.; Zhang, K.; Wang, X.; Xu, X. Development of green solvents for efficient post-combustion CO_2 capture with good regeneration performance. *J. CO2 Util.* **2022**, *59*, 101955–101962. [CrossRef]
47. Shohrat, A.; Zhang, M.; Hu, H.; Yang, X.; Liu, L.; Huang, H. Mechanism study on CO_2 capture by ionic liquids made from TFA blended with MEA and MDEA. *Int. J. Greenh. Gas Control.* **2022**, *119*, 101955–101964. [CrossRef]

48. Hou, H.; Jiao, B.; Li, Q.; Lin, X.; Liu, M.; Shi, H.; Wang, L.; Liu, S. Physicochemical properties, NMR, Ab initio calculations and the molecular interactions in a binary mixture of N-methylimidazole and water. *J. Mol. Liq.* **2018**, *257*, 100–111. [CrossRef]
49. Wang, L.; Liu, S.; Wang, R.; Li, Q.; Zhang, S. Regulating Phase Separation Behavior of a DEEA-TETA Biphasic Solvent Using Sulfolane for Energy-Saving CO_2 Capture. *Environ. Sci. Technol.* **2019**, *53*, 12873–12881. [CrossRef]
50. Kariznovi, M.; Nourozieh, H.; Abedi, J. Experimental measurements and predictions of density, viscosity, and carbon dioxide solubility in methanol, ethanol, and 1-propanol. *J. Chem. Thermodyn.* **2013**, *57*, 408–415. [CrossRef]
51. Jing, G.; Liu, F.; Lv, B.; Zhou, X.; Zhou, Z. Novel Ternary Absorbent: Dibutylamine Aqueous–Organic Solution for CO_2 Capture. *Energy Fuels* **2017**, *31*, 12530–12539. [CrossRef]
52. Min, K.; Choi, W.; Kim, C.; Choi, M. Oxidation-stable amine-containing adsorbents for carbon dioxide capture. *Nat. Commun.* **2018**, *9*, 726–732. [CrossRef] [PubMed]
53. Nwaoha, C.; Idem, R.; Supap, T.; Saiwan, C.; Tontiwachwuthikul, P.; Rongwong, W.; Al-Marri, M.J.; Benamor, A. Heat duty, heat of absorption, sensible heat and heat of vaporization of 2–Amino–2–Methyl–1–Propanol (AMP), Piperazine (PZ) and Monoethanolamine (MEA) tri–solvent blend for carbon dioxide (CO_2) capture. *Chem. Eng. Sci.* **2017**, *170*, 26–35. [CrossRef]
54. Wang, R.; Liu, S.; Li, Q.; Zhang, S.; Wang, L.; An, S. CO_2 capture performance and mechanism of blended amine solvents regulated by N-methylcyclohexyamine. *Energy* **2021**, *215*, 119209–119217. [CrossRef]
55. Chen, Z.; Jing, G.; Lv, B.; Zhou, Z. An Efficient Solid–Liquid Biphasic Solvent for CO_2 Capture: Crystalline Powder Product and Low Heat Duty. *ACS Sustain. Chem. Eng.* **2020**, *8*, 14493–14503. [CrossRef]
56. Chen, S.; Chen, S.; Fei, X.; Zhang, Y.; Qin, L. Solubility and Characterization of CO_2 in 40 mass % N-Ethylmonoethanolamine Solutions: Explorations for an Efficient Nonaqueous Solution. *Ind. Eng. Chem. Res.* **2015**, *54*, 7212–7218. [CrossRef]
57. Liu, S.; Ling, H.; Lv, J.; Gao, H.; Na, Y.; Liang, Z. New Insights and Assessment of Primary Alkanolamine/Sulfolane Biphasic Solutions for Post-combustion CO_2 Capture: Absorption, Desorption, Phase Separation, and Technological Process. *Ind. Eng. Chem. Res.* **2019**, *58*, 20461–20471. [CrossRef]
58. Wang, M.; Wang, M.; Rao, N.; Li, J.; Li, J. Enhancement of CO_2 capture performance of aqueous MEA by mixing with [NH_2e-mim][BF_4]. *RSC Adv.* **2018**, *8*, 1987–1992. [CrossRef]
59. Nwaoha, C.; Saiwan, C.; Tontiwachwuthikul, P.; Supap, T.; Rongwong, W.; Idem, R.; Al-Marri, M.J.; Benamor, A. Carbon dioxide (CO_2) capture: Absorption-desorption capabilities of 2-amino-2-methyl-1-propanol (AMP), piperazine (PZ) and monoethanolamine (MEA) tri-solvent blends. *J. Nat. Gas Sci. Eng.* **2016**, *33*, 742–750. [CrossRef]
60. Liu, F.; Fang, M.; Dong, W.; Wang, T.; Xia, Z.; Wang, Q.; Luo, Z. Carbon dioxide absorption in aqueous alkanolamine blends for biphasic solvents screening and evaluation. *Appl. Energy* **2019**, *233–234*, 468–477. [CrossRef]
61. Li, X.; Zhou, X.; Wei, J.; Fan, Y.; Liao, L.; Wang, H. Reducing the energy penalty and corrosion of carbon dioxide capture using a novel nonaqueous monoethanolamine-based biphasic solvent. *Sep. Purif. Technol.* **2021**, *265*, 118481–118488. [CrossRef]
62. Bai, L.; Lu, S.; Zhao, Q.; Chen, L.; Jiang, Y.; Jia, C.; Chen, S. Low–energy–consuming CO_2 capture by liquid–liquid biphasic absorbents of EMEA/DEEA/PX. *Chem. Eng. J.* **2022**, *450*, 138490–138500. [CrossRef]
63. Gao, X.; Li, X.; Cheng, S.; Lv, B.; Jing, G.; Zhou, Z. A novel solid–liquid 'phase controllable' biphasic amine absorbent for CO_2 capture. *Chem. Eng. J.* **2022**, *430*, 132932–132943. [CrossRef]
64. Zhang, R.; Liang, Z.; Liu, H.; Rongwong, W.; Luo, X.; Idem, R.; Yang, Q. Study of Formation of Bicarbonate Ions in CO_2-Loaded Aqueous Single 1DMA2P and MDEA Tertiary Amines and Blended MEA–1DMA2P and MEA–MDEA Amines for Low Heat of Regeneration. *Ind. Eng. Chem. Res.* **2016**, *55*, 3710–3717. [CrossRef]
65. Zhang, X.; Zhang, R.; Liu, H.; Gao, H.; Liang, Z. Evaluating CO_2 desorption performance in CO_2-loaded aqueous tri-solvent blend amines with and without solid acid catalysts. *Appl. Energy* **2018**, *218*, 417–429. [CrossRef]